
Article:
Bernal, S.A., Provis, J.L. orcid.org/0000-0003-3372-8922, Myers, R.J. et al. (2 more authors) (2015) Role of carbonates in the chemical evolution of sodium carbonate-activated slag binders. Materials and Structures, 48 (3). pp. 517-529. ISSN 1359-5997

https://doi.org/10.1617/s11527-014-0412-6

Postprint of a paper published in *Materials and Structures*, 48(2015):517-529. Version of record is available at http://dx.doi.org/10.1617/s11527-014-0412-6

Role of carbonates in the chemical evolution of sodium carbonate-activated slag binders

Susan A. Bernal,[1] John L. Provis,[1]* Rupert J. Myers,[1] Rackel San Nicolas,[2] Jannie S.J. van Deventer[2,3]

[1]*Department of Materials Science and Engineering, The University of Sheffield, Sheffield S1 3JD, UK*

[2]*Department of Chemical & Biomolecular Engineering, The University of Melbourne, Victoria 3010, Australia*

[3]*Zeobond Pty Ltd, P.O. Box 210, Somerton, Victoria 3062, Australia*

*To whom correspondence should be addressed. Email j.provis@sheffield.ac.uk, phone +44 114 222 5490, fax +44 114 222 5493

Abstract

Multi-technique characterisation of sodium carbonate-activated blast furnace slag binders was conducted in order to determine the influence of the carbonate groups on the structural and chemical evolution of these materials. At early age (<4 days) there is a preferential reaction of Ca^{2+} with the CO_3^{2-} from the activator, forming calcium carbonates and gaylussite, while the aluminosilicate component of the slag reacts separately with the sodium from the activator to form zeolite NaA. These phases do not give the high degree of cohesion necessary for development of high early mechanical strength, and the reaction is relatively gradual due to the slow dissolution of the slag under the moderate pH conditions introduced by the Na_2CO_3 as activator. Once the CO_3^{2-} is exhausted, the activation reaction proceeds in similar way to an NaOH-activated slag binder, forming the typical binder phases calcium aluminium silicate hydrate and hydrotalcite, along with Ca-heulandite as a further (Ca,Al)-rich product. This is consistent with a significant gain in compressive strength and reduced porosity observed after 3 days of curing. The high mechanical strength and reduced permeability developed in these materials beyond 4 days of curing elucidate that Na_2CO_3-activated slag can develop desirable properties for use as a building materials, although the slow early strength development is likely to be an issue in some applications. These results suggest that the inclusion of additions which could control the preferential consumption of Ca^{2+} by the CO_3^{2-} might accelerate the reaction kinetics of Na_2CO_3-activated slag at early times of curing, enhancing the use of these materials in engineering applications.

Keywords: alkali-activated slag; sodium carbonate; X-ray diffraction; nuclear magnetic resonance; X-ray microtomography.

1. Introduction

Alkali-activated binders have been developed for over a century as a means for valorising industrial wastes and by-products, and to produce Portland clinker free cement-like materials to mitigate the environmental footprint associated with Portland cement manufacture [1, 2]. The production of alkali-activated binders offers a reduced embodied energy and significantly lower release of pollutant gases when compared with Portland cement, and these materials can develop comparable mechanical strength and performance when properly formulated and cured [3, 4]. The need to develop low-cost and low-environmental footprint alkali activated materials has motivated the identification and adoption of alkaline activators that can promote the development of high mechanical strength and reduced permeability in the binder, and achieve alkalinities comparable to those in Portland cement based materials, so that the metallic component of structural concrete is not excessively corroded during the service life.

The microstructure, and therefore the performance, of alkali-activated slag materials is strongly dependent on factors such as the chemistry and mineralogy of the slag precursor, the type and concentration of the alkali-activator and the curing conditions [5-10]. The commonly used activators for the production of activated slag binders are sodium hydroxide (NaOH), sodium silicates ($Na_2O{\cdot}rSiO_2$), sodium carbonate (Na_2CO_3) and sodium sulfate (Na_2SO_4) [6, 9, 11, 12]. It is well known that the effectiveness of the activator is based on its ability to generate an elevated pH, as this controls the initial dissolution of the precursor and the consequent condensation reaction to form the reaction products [13-15].

A high pH is expected to favour the dissolution of the slag to form strength-giving phases such as calcium aluminium silicate hydrate (C-A-S-H) type gels [16]. However, pH is not the only factor controlling the mechanism of reaction taking place when activating slag. It has been observed [17, 18] that using a sodium silicate activator, which has a lower pH than sodium hydroxide solutions, when dosed with equivalent Na_2O content, promotes the development of binders with higher mechanical strength. This is a consequence of the additional silicate species that it provides to the system, and the interparticle electrostatic forces governing the formation of the binder when using this activator [19]. This indicates that the functional group

accompanying the alkaline activator is playing an important role in the activation mechanism of these materials.

Sodium carbonate activation of blast furnace slag has been applied for half a century in Easter Europe [20, 21], as a lower cost and more environmentally friendly alternative to the widely used activators sodium hydroxide or sodium silicate used for production of activated slag products [22, 23]. More recent work on Na_2CO_3-slag-fine limestone concretes showed very good early strength development, and calculated potential Greenhouse emission savings as high as 97% compared to Portland cement [24-26]. The use of this activator forms binders with reduced pH compared with materials produced with NaOH and $Na_2O{\cdot}rSiO_2$ [27]. This is especially attractive for specialized applications such as the immobilisation of nuclear wastes containing reactive metals which corrode at high pH [27]. However, the understanding of the structural development of carbonate-activated slag is very limited, as carbonate-activated binders have attracted less attention than other activated-slag systems because of the delayed hardening (which can take up to 5 days in some systems) and slower strength development [28-30], when compared with other alkali-activated slag binders.

It has been identified [26, 29] that at early times of reaction of Na_2CO_3-activated slags form calcium and mixed sodium-calcium carbonates, as a consequence of the interaction of the CO_3^{2-} from the activator with the Ca^{2+} from the dissolved slag; however, longer times of curing favour the formation of C-A-S-H type gels. Xu et al. [21] evaluated aged slag activated with Na_2CO_3 and Na_2CO_3/NaOH blends, and identified as the main reaction product a highly crosslinked C-A-S-H type phase with a reduced content of Ca in the outer product, along with an inner product involving carbonate anions. Formation of Ca-Na mixed carbonates was not detected in aged Na_2CO_3-activated slag concretes, which differs from what has been identified in young (28-day) samples where gaylussite is often observed [26, 31].

It has been proposed [21] that in Na_2CO_3 activated slag binders the activation reaction takes place through a cyclic hydration process where the Na_2CO_3 supplies a buffered alkaline environment where the level of CO_3^{2-} available in the system is maintained by the continual dissolution of $CaCO_3$ in equilibrium with the pore solution, releasing Ca^{2+} to react with the dissolved silicate from the slag to form C-S-H type products. However, there is not yet detailed evidence of how this mechanism might be established and then proceed over the first months of reaction in Na_2CO_3-activated slags.

In this study the structural evolution of sodium carbonate activated slag pastes is assessed through X-ray diffraction, ^{29}Si and ^{27}Al MAS NMR spectroscopy and X-ray microtomography. Isothermal calorimetry of fresh paste is also conducted in order to determine the kinetic of reaction of sodium carbonate pastes. Compressive strength values of mortars corresponding to the pastes produced for the structural study are reported in order to develop a better understanding of the relationship between the structural characteristics of these binders and their mechanical strength development.

2. Experimental program

2.1. Materials and sample preparation

As primary raw material a granulated blast furnace slag (GBFS) was used, supplied by Zeobond Pty Ltd., Australia, with oxide composition as shown in Table 1. Its specific gravity is 2800 kg/m^3 and Blaine fineness 410±10 m^2/kg. The particle size range, determined through laser granulometry, was 0.1-74 μm, with a d_{50} of 15 μm.

Table 1. Composition of GBFS used. LOI is loss on ignition at 1000°C

Component (mass % as oxide)	GBFS
SiO_2	33.8
Al_2O_3	13.7
Fe_2O_3	0.4
CaO	42.6
MgO	5.3
Na_2O	0.1
K_2O	0.4
Others	1.9
LOI	1.8

Commercial sodium carbonate (Sigma-Aldrich) was dissolved in the mix water until complete dissolution was reached. The assessment of structural evolution was conducted in paste specimens formulated with a water/binder ratio of 0.40 and an activator (Na_2CO_3) content of 8

wt.% relative to the amount of slag for strength development, NMR, XRD and calorimetry analysis, and 7 wt.% for microtomography. All paste specimens were cured in sealed centrifuge tubes at 23°C until testing. Mortar cubes, 50 mm in size, were used for compressive strength testing; these were formulated with a sand:binder ratio of 2:75, and a binder formulation matching the paste specimens.

Isothermal calorimetry experiments were conducted using a TAM Air isothermal calorimeter, at a base temperature of 25 ± 0.02°C. Fresh paste was mixed externally, weighed into an ampoule, and immediately placed in the calorimeter, and the heat flow was recorded for the first 140 h of reaction. All values of heat release rate are normalised by total weight of paste.

2.2. Tests conducted on hardened specimens

The hardened paste specimens were analysed after periods of up to 45 days of curing through:

- Compressive strength testing, using an ELE International Universal Tester, at a loading rate of 1.0 kN/s for the 50 mm mortar cubes.
- X-ray diffraction (XRD), using a Bruker D8 Advance instrument with Cu Kα radiation and a nickel filter. The tests were conducted with a step size of 0.020º, over a 2θ range of 5º to 70º.
- Magic angle spinning nuclear magnetic resonance (MAS NMR) spectroscopy; ^{29}Si MAS NMR spectra were collected at 119.1 MHz on a Varian INOVA-600 (14.1 T) spectrometer using a probe for 4 mm o.d. zirconia rotors and a spinning speed of 10.0 kHz. The ^{29}Si MAS experiments employed a pulse width of 6 µs, a relaxation delay of 60 s and 4300-6500 scans. Solid-state ^{27}Al MAS NMR spectra were acquired at 156.3 MHz on the same instrument, with a pulse width of 6 µs, a relaxation delay of 2 s. All the spectra were collected with a pulse angle of 51º. ^{29}Si and ^{27}Al chemical shifts are referenced to external samples of tetramethylsilane (TMS) and a 1.0 M aqueous solution of $AlCl_3.6H_2O$, respectively.
- Samples cured for up to 45 days and ~1 mm in size were analysed using beamline 2-BM at the Advanced Photon Source, Argonne National Laboratory [32]. Reactions were halted after the specified curing duration by immersion of the samples in acetone until testing, and analytical specimens were taken from the part of the sample close to the interface between solid material and acetone to ensure that the reaction had been halted promptly in

the sections use for testing. Measurements were carried out using hard X-ray synchrotron radiation (22.5 keV) in a parallel-beam configuration, with 0.12° rotation per step (1501 steps in a 180° rotation) and 0.4 s exposure time per step. Samples were mounted in small polymeric cones to enable alignment; sample size and shape were somewhat irregular, as the samples were obtained by fracturing larger monoliths, but all samples fitted within the field of view in the horizontal plane of the detector. X-ray detection was achieved with a scintillator and CCD camera, capturing 2048×2048 pixels. Tomographic data were reconstructed using an in-house developed reconstruction algorithm, including recentring following visual inspection to ensure optimal reconstructions, using a voxel size of 0.75 μm (corresponding to the detector resolution). The segmentation, pore connectivity and tortuosity calculations on volume of interest (VOI) regions of at least 400 pixels^3 were performed following the protocol described in [33].

3. Results and discussion

3.1. Compressive strength

The compressive strength of sodium carbonate activated slag mortars could not be determined at 1 day because the material was still soft. However, after 4 days the mortars gained a compressive strength of 9 MPa (Figure 1), followed by a substantial rise in the subsequent 3 days to reach 31 MPa after 7 days of curing. This compressive strength gain indicates that the initial mechanism of reaction in sodium carbonate activated slag binders is not leading to the formation of strength-giving phases during the first days of curing, and consequently the samples are not developing a measurable compressive strength during this time. Subsequently, there is an increase in the formation of strength-giving phases from 4 to 7 days, with an associated jump in strength. After this, there is an ongoing gradual increase in the compressive strength with extended curing (up to 44 MPa at 56 days).

Postprint of a paper published in *Materials and Structures*, 48(2015):517-529. Version of record is available at http://dx.doi.org/10.1617/s11527-014-0412-6

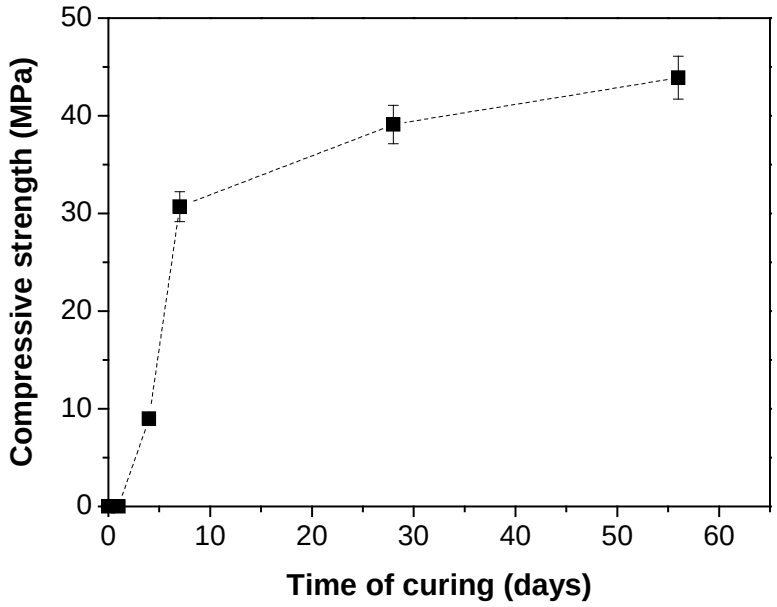

Figure 1. Compressive strength of sodium carbonate-activated slag binders as a function of the time of curing

3.2. Isothermal calorimetry

The heat release curves of the sodium carbonate activated slag are shown in Figure 2. There is an initial pre-induction period, associated with the partial dissolution of the slag particles, in the first 48 h, followed by an extended induction period (~62 h) where little heat evolution is taking place. This is consistent with the fact that hardening is observed to take place slowly during the first 4 days of curing in these samples. Extended induction periods in sodium carbonate activated slag binders have also been observed by Fernandez-Jimenez et al. [34]; however, in that study the precipitation of reaction products was observed via an acceleration in heat release 6 hours after mixing, rather than after several days here. The differences in the results between studies can be mainly attributed to the differences in the chemistry of the slag (mainly the MgO content), as the specific surface and amorphous content of the material used in that work seem to be similar to the slag used in the present study. The MgO content of slag has recently been identified to play a key role in defining the nature of the reaction products in alkali-activated slag binders [35], and this is the main identifiable difference between the two binder systems.

Postprint of a paper published in *Materials and Structures*, 48(2015):517-529. Version of record is available at http://dx.doi.org/10.1617/s11527-014-0412-6

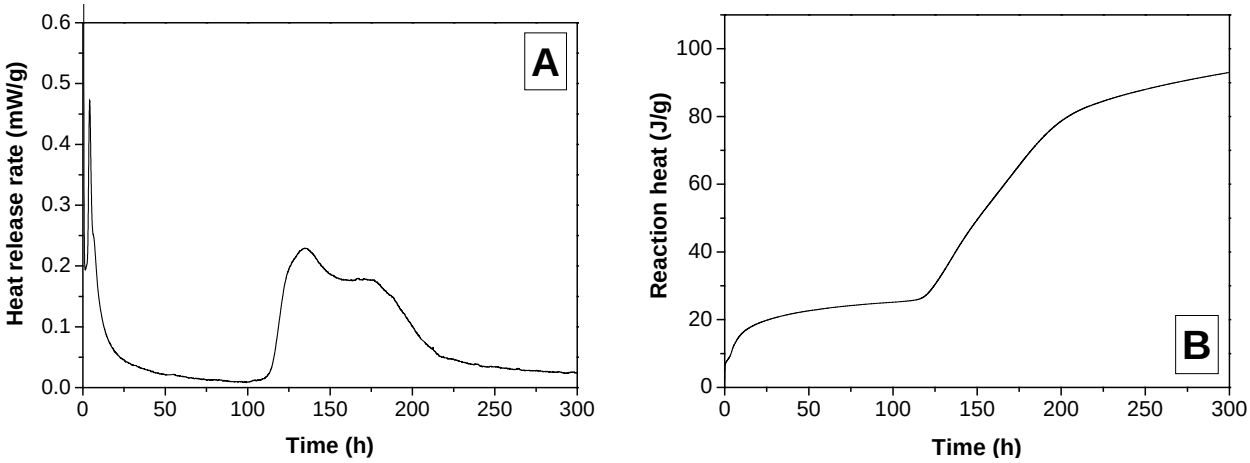

Figure 2. (A) Heat release rate and (B) cumulative heat release of sodium carbonate-activated slag binders

After the induction period, a high intensity heat evolution process, corresponding to the processes generally described as the acceleration and deceleration periods in cementitious binders (~110-220 h) is identified. This peak corresponds to the precipitation of voluminous reaction products in the binder, releasing a significant heat of reaction. In this case the heat release seems to be occurring in two consecutive stages, as two clear maximum heat release peaks are observed in Figure 2A. The occurrence and timing of the acceleration-deceleration period agree well with the increase in compressive strength observed in these specimens (Figure 1) at a similar time of curing, confirming that the formation of the bulk binding phases responsible for both strength and heat output is not taking place during the first 3 days of reaction. This is to a significant extent consistent with the very moderate initial pH of these binders, as it takes time for the pH to increase to the point where the slag will start to react rapidly to form these binding phases.

These results different from those identified in sodium silicate activation of this same slag [35], and in other systems with comparable slag chemistry [18], where the pre-induction period was observed during the first hours of reaction, followed by short induction periods (<10 h in metasilicate activated slags with MgO contents lower than 8 wt.% [35]). However, it has been noted [36], that in sodium metasilicate activation of slags with reduced alumina (11.9 wt.%) content, the induction period was as long as 6 days. This elucidates that delayed precipitation of reaction products is not an exclusive effect of the nature of the alkaline activator, but also relates to the chemical and mineralogical composition of the slag used.

Postprint of a paper published in *Materials and Structures*, 48(2015):517-529. Version of record is available at http://dx.doi.org/10.1617/s11527-014-0412-6

3.3. X-ray diffraction

The evolution of crystalline phases forming in a sodium carbonate activated slag is shown in Figure 3. In samples cured for one day the main crystalline compounds forming are the three polymorphs of calcium carbonate ($CaCO_3$): calcite (powder diffraction file, PDF #005-0586), vaterite (PDF #002-0261) and aragonite (PDF #04-013-9616), along with the double salt gaylussite ($Na_2Ca(CO_3)_2 \cdot 5H_2O$, PDF #021-0343) and zeolite NaA ($Na_{12}Al_{12}Si_{12}O_{48} \cdot 18H_2O$, PDF#039-0221). Formation of calcium carbonate in various polymorphs, and gaylussite, has been identified in carbonated alkali-activated slag binders [37, 38]. The identification of similar reaction products in the carbonate-activated binder suggests that there is a preferential early age reaction between dissolved CO_3^{2-} present in the pore solution and the Ca^{2+} released by the partial dissolution of the slag. The consumption of Ca^{2+} by CO_3^{2-} then leads to a saturation of Si and Al species with respect to aluminosilicate type products such as zeolite NaA in the NaOH-rich pore solution from the very earliest stages of the reaction process.

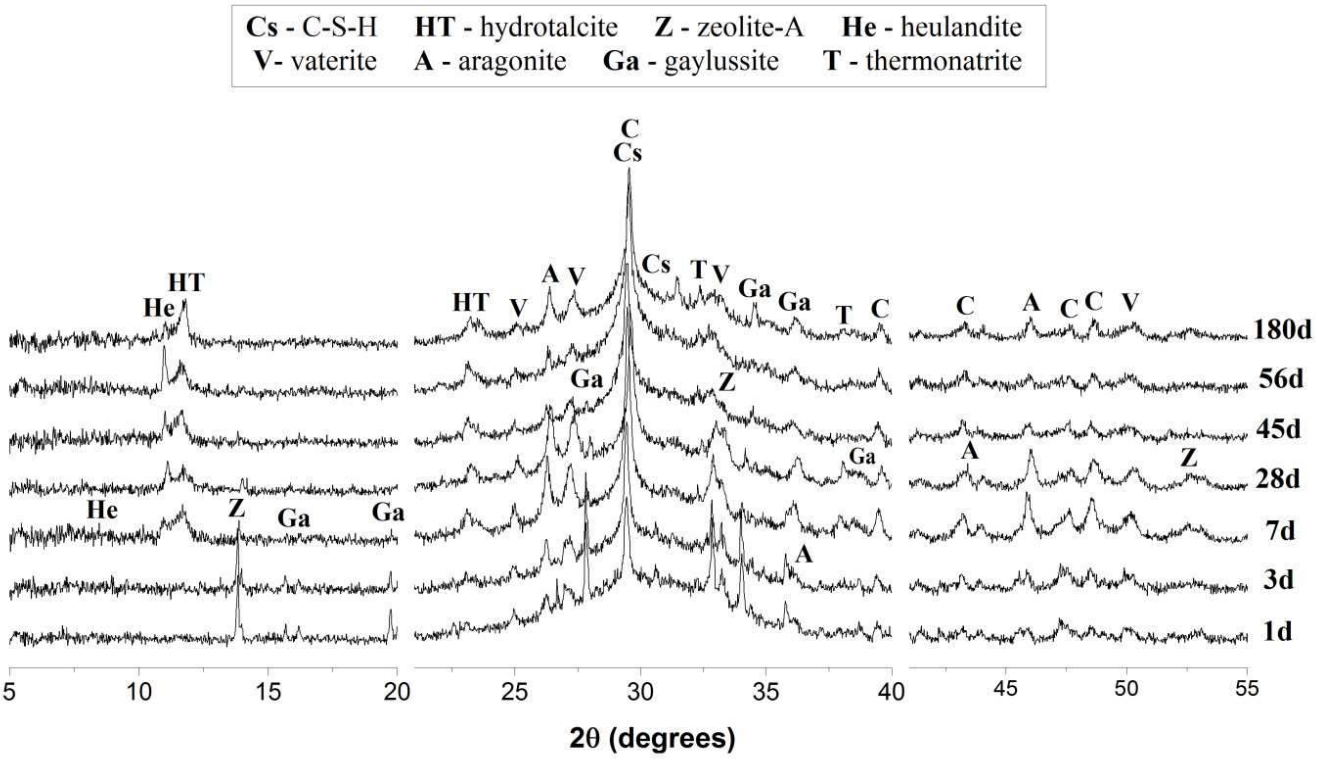

Figure 3. X-ray diffractograms of sodium carbonate-activated slag binders as a function of the time of curing, as shown.

After 7 days of curing, the intensities of the zeolite NaA and gaylussite peaks have decreased; these phases are almost fully consumed by 45 days. Instead, the Ca-containing zeolite

heulandite (approximately $CaAl_2Si_7O_{18}\cdot nH_2O$, n = 3.5 to 6, PDF# 025-0144 or 024-0765) and a calcium aluminium silicate hydrate (C-A-S-H) (resembling a disordered, Al-substituted form of tobermorite-11Å, $Ca_5Si_6O_{18}\cdot 5H_2O$, PDF #045-1480), and a layered double hydroxide with a hydrotalcite type structure ($Mg_6Al_2CO_3(OH)_{16}\cdot 4H_2O$, PDF# 014-0191), are observed. Heulandite has been identified as a secondary reaction product in preparation of synthetic C-A-S-H phases with 30% silicon replacement by aluminium [39] and in aged (7 years) silicate-activated slag binders [40], while C-A-S-H products along with hydrotalcite are the main reaction products forming in alkali-activated slags produced with either NaOH or $Na_2O.rSiO_2$ [18, 31, 37, 41]. The formation of these reaction products indicates that once the CO_3^{2-} supplied by the alkaline activator is largely consumed in the formation of carbonate compounds, which is likely to be the case after a few days of reaction, the mechanism of reaction of sodium-carbonate activated slags proceeds in the same way as in sodium hydroxide-activated or sodium silicate-activated systems. This is in good agreement with the rise in the mechanical strength identified in these samples at this time.

Traces of thermonatrite ($Na_2CO_3\cdot H_2O$) are identified in all samples after 28 or more days of curing, which suggest that this is not simply a dried remnant of the remnant activator in the pore solution, as it is not observed in the younger samples. Instead, thermonatrite is likely to be a product derived from the carbonation of the pore solution during exposure to ambient air for XRD analysis, as it has also been identified in carbonated metasilicate-activated slags [35, 37, 42]. Significant increases in the intensities of the reflections assigned to heulandite, hydrotalcite and C-A-S-H are observed at advanced times of curing; however, it seems that after 180 days, the systems is mainly dominated by hydrotalcite and C-A-S-H, with traces of sodium and calcium carbonate compounds. Gaylussite appears to have been converted entirely to more stable products. An extended period of formation of these reaction products is controlling the ongoing compressive strength gain observed in these binders (Figure 1).

3.4. Nuclear Magnetic Resonance

The ^{29}Si MAS NMR spectra of the anhydrous slag and sodium carbonate-activated binders (Figure 4A) show little change after 1 day of curing, consistent with a relatively slow rate of reaction of the slag. However, a low intensity peak is observed at -83 ppm, consistent with a $Q^2(1Al)$ site characteristic of the Al substituted C-S-H type phase which forms in alkali-activated slags [35, 37, 43], which suggests that the preferential formation of carbonates is not completely hindering the formation of this product. In this spectrum it is also possible to

Postprint of a paper published in *Materials and Structures*, 48(2015):517-529. Version of record is available at http://dx.doi.org/10.1617/s11527-014-0412-6

identify a shoulder at -89.5 ppm which corresponds to the presence of zeolite NaA [44], which becomes less prominent beyond 7 d as the prevalence of this phase decreases. There is no clear peak due to heulandite observable (in the region around -100 ppm [45]) at longer ages, but the concentration of this phase is always low according to XRD also.

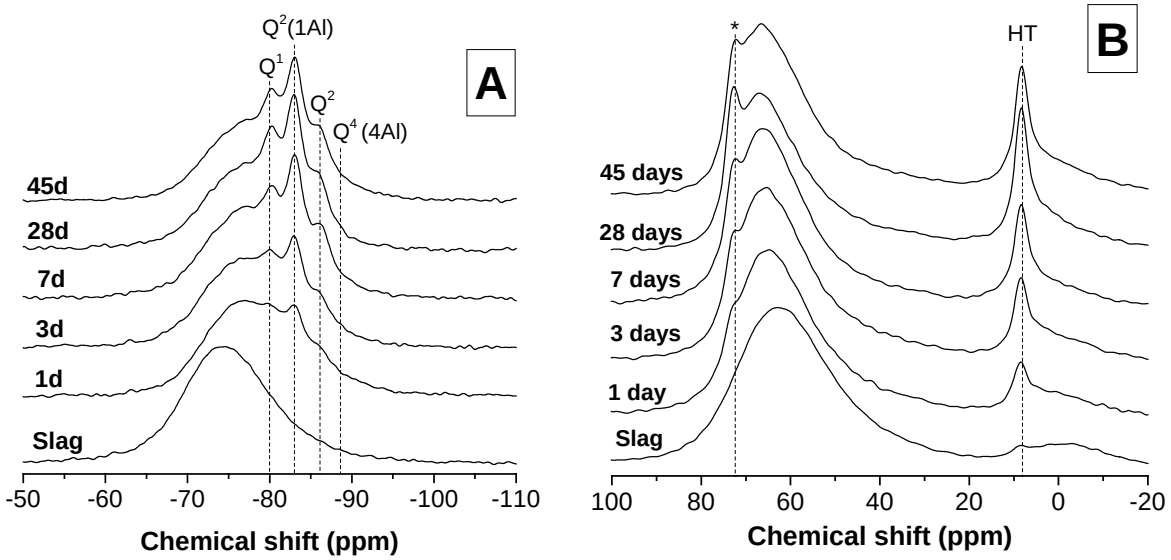

Figure 4. (A) ^{29}Si and (B) ^{27}Al MAS NMR spectra of sodium carbonate-activated slag binders as function of the time of curing. HT is hydrotalcite, and the asterisk corresponds to Al in Q^2 sites in the C-A-S-H phase

At increased times of reaction, the formation of sites at -80 ppm, -83 ppm and -86 ppm, corresponding to the Q^1, Q^2(1Al) and Q^2 species in C-A-S-H products [46, 47], becomes increasingly clear. A higher intensity of these sites is observed with increasing curing time, consistent with the higher intensity of the C-A-S-H phase reflections identified by XRD (Figure 3), and the increased strength of the binders over the time of curing (Figure 1). Complicating any quantitative analysis of these spectra is an apparently partially-selective reaction of the slag, which means that direct subtraction of an unreacted component from the spectra – which is a prerequisite for any useful deconvolution – is unfortunately not possible. This partial selectivity is evident from observation of the region around -65 to -70 ppm in Figure 4A, where the signal in this region corresponds to the highly depolymerised (Q^0) silicate component within the slag glass. Because these sites in the slag are able to be released without the need to break any of the relatively strong Si-O-Al or Si-O-Si network bonds, they are able to be selectively leached under the relatively mild pH conditions prevailing early in the reaction

process here. Slag dissolution in alkali-activated systems is often assumed to be congruent [35, 48-50], and this is consistent with the dissolution taking place rapidly under far-from-equilibrium conditions where Si-O-(Si,Al) bonds can readily be broken. However, at a more moderate pH and in the presence of carbonate, which is driving the extraction of calcium from the slag glass, the Q^0 sites would logically be prone to preferential release. This is observed in the spectra in Figure 4A by the fact that the region from -65 to -70 ppm decreases significantly in intensity within the first day of reaction. After this time, there is little additional change in this part of the spectra, suggesting that the slag dissolution proceeds close to congruently beyond this point.

Three distinct types of aluminium environments, Al(IV) (52-80 ppm), Al(V) (30-40 ppm) and Al(VI) (0-20 ppm) [51], are identified in all of the ^{27}Al MAS NMR spectra. Figure 4B shows sharpening in the tetrahedral Al band after 7 d of curing compared with the unreacted slag, along with the formation of a narrow peak at 74 ppm, whose intensity increases with curing time. This band is assigned to the Al(IV) incorporated in bridging tetrahedra bonded to Q^2(1Al) sites in the C-A-S-H [39, 47]. After 28 days of curing, asymmetric broadening of the band at 68 ppm is observed, along with the formation of a low intensity shoulder at ~58 ppm, consistent with the formation of Al-substituted tobermorites with low Ca/(Si+Al) ratio [39]. Small contributions of the zeolite heulandite identified by XRD (Figure 3) are expected at around 63 ppm, [52], and the band at 62 ppm whose intensity seems to be higher at advanced times of curing is consistent with this phase. At extended times of curing, the formation of a narrow peak centred at 8.7 ppm is also observed. This peak corresponds to the hydrotalcite type phases, and the increased intensity of this band over the time of curing is consistent with the XRD data (Figure 3).

3.5. X-ray microtomography (μCT)

High resolution X-ray microtomography (μCT) has been proven to be a suitable technique for the study of pore structure and tortuosity in alkali-activated binders [33] and in Portland cement materials [53, 54], via segmentation of the samples into pore and solid regions to identify pore geometry and tortuosity. The calculation of the porosity and tortuosity here follows the methodology detailed in [33], and the results for samples of different ages are shown in Figure 5.

Postprint of a paper published in *Materials and Structures*, 48(2015):517-529. Version of record is available at http://dx.doi.org/10.1617/s11527-014-0412-6

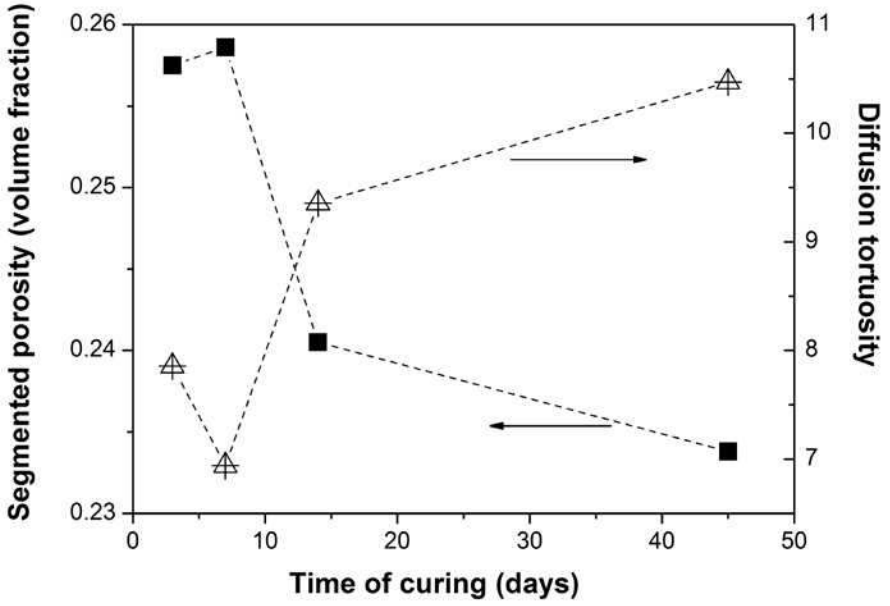

Figure 5. Segmented porosity and diffusion tortuosity of sodium carbonate-activated slag binders as function of the time of curing. Estimated uncertainty is ±3% of the porosity (i.e. around ±0.005 in the porosity fractions plotted here), and ±0.5 units in tortuosity.

The porosity values (Figure 5) decrease with increasing curing duration, and fall within a similar range to the values published in [33] for sodium metasilicate-activated slag binders of comparable mix design. The porosities at 14 and 45 days in the sodium carbonate-activated specimens here are around 10% lower than the corresponding data for the silicate-activated binders in [33], which were of similar mix designs. It is likely that the apparent increase in porosity in the 7-day sample (and corresponding drop in tortuosity) actually falls within experimental uncertainty for the expected monotonic behaviour; there is not a good microstructural explanation for a temporary increase in porosity at this time.

The diffusion tortuosity values of these specimens are notably higher than the values measured for silicate-activated slag or slag-fly ash blends in [33]. The highest tortuosity determined in that study was for the sodium metasilicate-100% slag binder at 45 days, which had a tortuosity of 8. The sodium carbonate-activated slag binder here exceeds that value by 14 days of age, and reaches a value of more than 10 by 45 days. This may be important for long term durability, because diffusion tortuosity is defined as the ratio of the rate of diffusion of a species in free space to its rate of diffusion within the material. This means that the diffusion tortuosity can be interpreted as being related to the resistance to transport through the material by diffusive

mechanisms, and is therefore a key factor controlling the service life of a reinforced concrete element.

The decrease in porosity and increase in tortuosity as a function of curing duration is also consistent with the results for slag-rich alkali-activated binders, where this trend is attributed to the growth of C-S-H type binding products which incorporate and chemically bind water. Such products are formed in the Na_2CO_3-activated binders after the initial consumption of carbonate from the activator has taken place, the dissolved carbonate concentration is low, and so the Ca^{2+} released by further slag dissolution is free to react with silicates instead.

3.6. Scanning electron microscopy

A backscattered electron (BSE) image of 1-day cured Na_2CO_3 activated slag paste (Figure 6A) shows a highly porous (black regions) and heterogeneous matrix (main grey region) with embedded large angular particles (light grey) corresponding to unreacted slag. This microstructure is consistent with the limited mechanical strength (Figure 1) and high porosity (Figure 5) identified at early age. Conversely, after 56 days of curing (Figure 6B), the material develops a cohesive and relatively homogeneous continuous matrix, in agreement with the formation of space-filling reaction products such as C-A-S-H type gel, as previously identified via XRD and NMR spectroscopy (Figures 3 and 4, respectively).

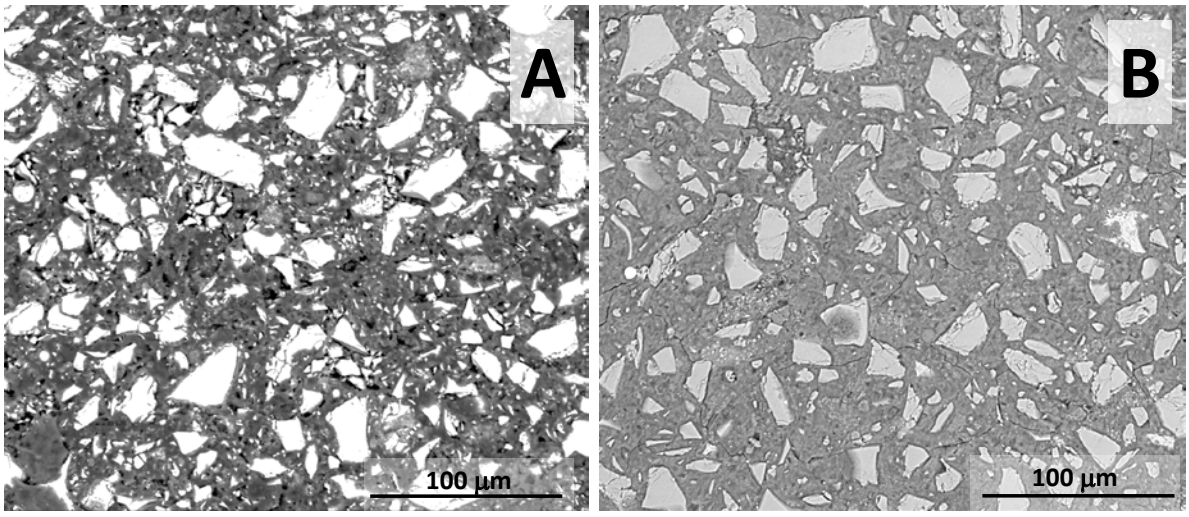

Figure 6. Backscattered electron images of alkali carbonate-activated slag binders after (A) 1 day and (B) 56 days of curing

EDX results for multiple points selected within the binder regions (i.e. excluding unreacted precursor particles) over the time of curing are shown in Figure 7. The Ca/Si vs Al/Si plot shows that the Al-substituted C-S-H type gel must be intimately intermixed with additional Al-rich products, as the Al/Si ratio is very high for a pure chain-structured C-A-S-H type phase, and is too high to show any notable degree of crosslinking [49]. This identification of additional products is consistent with the identification of Al-rich zeolites and hydrotalcite-like layered double hydroxides as secondary phases in these binders. The slope of the Mg/Si vs Al/Si plot gives information regarding the overall composition of the layered double hydroxide phase, which is seen to have an Mg/Al ratio of approximately 2 from these measurements. The data appear to indicate a greater degree of consistency in Ca/Si ratio with increased curing time (Figure 7A), as the gel is maturing and becoming more homogeneous as the binder develops.

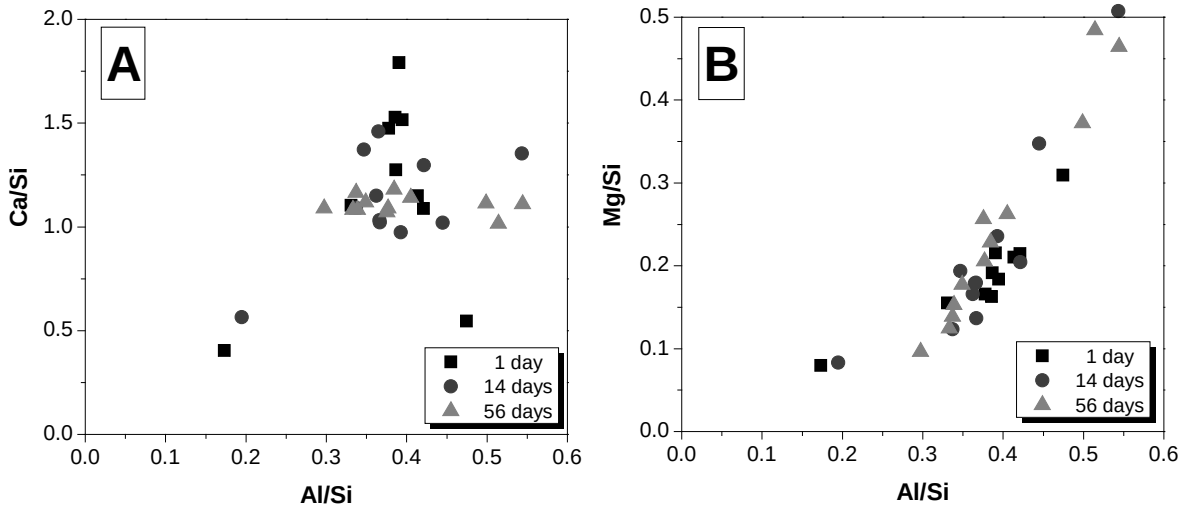

Figure 7. Atomic ratios (A) Ca/Si vs Al/Si and (B) Mg/Si vs Al/Si for bulk sodium carbonate activated slag paste as function of curing duration

3.7. Proposed conceptual description of the chemical mechanism of sodium carbonate-activation reaction

Based on the analytical results presented in this paper, and consistent with the known mechanical and chemical evolution of alkali-carbonate activated slag binders up to very extended ages [21], it is now possible to propose a detailed reaction mechanism for this reaction process. Figure 8 describes, in a purely conceptual sense, the proposed evolution of the binder chemistry according to three stages during which the changes in pore fluid chemistry are able to influence and control the solid phase assemblage which is forming, as follows.

Postprint of a paper published in *Materials and Structures*, 48(2015):517-529. Version of record is available at http://dx.doi.org/10.1617/s11527-014-0412-6

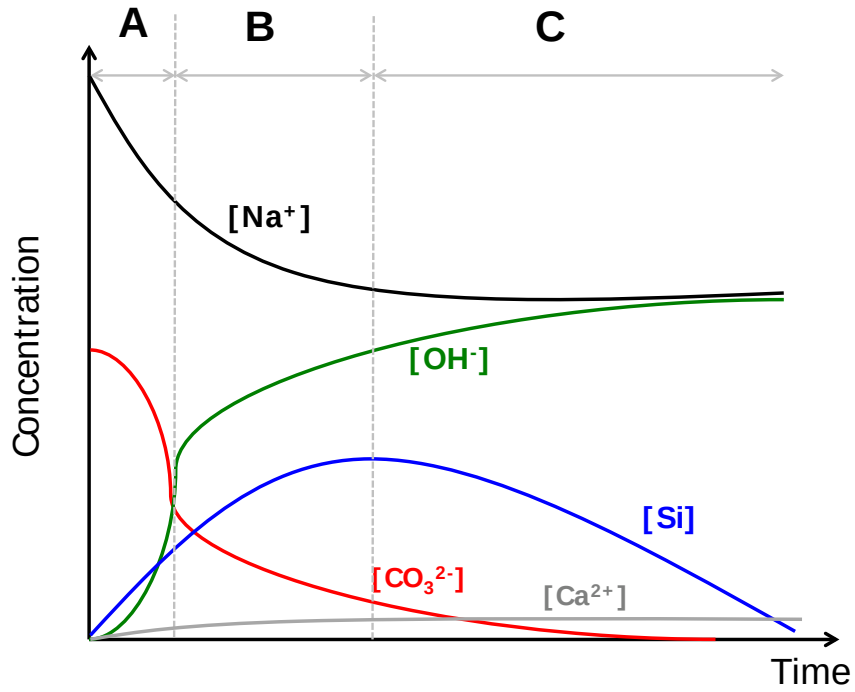

Figure 8. Proposed conceptual description of the pore solution chemistry within a sodium carbonate-activated slag binder. The stages of the reaction process are described in detail in the text; stage A is approximately the first day after mixing, stage B is the period up to approximately 5 days corresponding to the induction period in isothermal calorimetry, and stage C is the period beyond this, when calcium silicate-based binder phases are forming from solution. The concentration axis scale is arbitrary, probably approximately 0-2 mol/L but intended as indicative only.

Stage A (~day 1):

- Initial dissolution of slag, with heat release (pre-induction in calorimetry)
- Na_2CO_3 reacts with Ca^{2+} from slag to form gaylussite ($Na_2Ca(CO_3)_2 \cdot 5H_2O$)
- Si and Al from slag react with Na^+ to form zeolite A (Si/Al = 1.0)
- Dissolved OH^- and Si concentrations increasing

Stage B (~days 1 to 5-7):

- Induction period in calorimetry, dissolution of slag continuing
- Gaylussite converts to $CaCO_3$ and releases Na^+
- Zeolite phase Si/Al ratio seems to increases, with zeolite NaA replacement by heulandite commencing

- Extra Al forms hydrotalcite with Mg^{2+} from slag
- Dissolved OH^- and Si concentrations still increasing

Stage C (days 5-7 onwards):

- Precipitation of bulk C-A-S-H gel, heat release in calorimetry
- Reduction of CO_3^{2-} concentration in solution, with a slight increase in Ca^{2+} (as its solubility is no longer limited by saturation with respect to $CaCO_3$ polymorphs), promotes precipitation of C-A-S-H instead of $CaCO_3$ and reduces porosity
- Dissolved Si concentration decreases with C-A-S-H formation; OH^- concentration continues to increase and gives a highly alkaline pore solution (essentially NaOH) in the hardened binder, which continues to react with the slag
- Mg^{2+} continues to form hydrotalcite with Al
- Zeolite formation slows notably after replacement of NaA by heulandite is complete

This reaction mechanism is therefore able to explain the chemistry of binder formation in the alkali-activation of slag in a carbonate environment. The ongoing release of Ca, Si, Al and Mg from the slag particles leads to the progressive reduction in porosity observed in Figure 6. The relatively similar Ca/Si ratios between inner and outer products observed by Sakulich et al. [25] in 20 month-old Na_2CO_3-slag pastes are also consistent with a mechanism whereby the slag is essentially reacting with an NaOH solution at greater ages, as there is no region which is preferentially enriched with silica, the Mg and some of the Al are being consumed in hydrotalcite formation, and the carbonate has already precipitated as $CaCO_3$.

From this basis, it is possible to draw implications regarding the design and optimisation of binders based on alkali carbonate-activated slags. These are the potentially most cost-effective and environmentally-friendly of all alkali-activated systems due to the much simpler and less damaging process of production of Na_2CO_3 compared to the common industrial routes to NaOH or sodium silicate production. They can generate excellent strength after 7 or 28 days of curing, but the setting and hardening reactions of the systems studied here is not sufficiently rapid for the materials to serve as a practical cementing binder system in general applications. What seems to be required, to accelerate this process, would be a mechanism by which the carbonate can be removed from solution at early age, leaving the slag to then react in a NaOH-rich environment. There is therefore a need to develop such methods to manipulate the early age pore solution chemistry of these materials, either through the use of solid or liquid

additives, to achieve this early-age binding of carbonate and thus elevated pH. The new chemical understanding which has been developed in this paper will potentially hold the keys to the next steps of development in this area, to make these binders into a viable system of engineering materials for large-scale construction.

4. Conclusions

This paper has presented a detailed chemical and microstructural analysis of the mechanisms of phase formation and strength development in sodium carbonate-activated slag binders. These materials have been proposed as a low-CO_2 cementing binder system but tend to show slow strength development, which has to some extent restricted the level of scientific analysis which has been undertaken to date. However, the ability to understand and describe the mechanisms by which these systems do react offers the scope for future developments and optimisation of strength development performance, and so the results presented here are an initial step towards enabling the further development and more widespread deployment of materials based on this type of chemistry.

From analysis of the materials by diffractometry and spectroscopy, the phase evolution of these materials, involving the initial precipitation of carbonates and zeolites (during the pre-induction period as observed by calorimetry), with later development of C-A-S-H type phases (the acceleration-deceleration period), has been elucidated. In the first days of reaction, the carbonate supplied by the activator consumes essentially all of the calcium released by slag dissolution; it is only when this carbonate is largely consumed that the formation of C-A-S-H commences. The application of X-ray microtomography shows a significant ongoing decrease in porosity at extended times of curing, resulting in a high-strength binder with a particularly tortuous pore network, which is likely to be highly desirable for engineering applications if the early-age strength evolution can be enhanced.

Acknowledgements

This work has been funded by the Australian Research Council, through a Linkage Project cosponsored by Zeobond Pty Ltd, including partial funding through the Particulate Fluids Processing Centre. We wish to thank Adam Kilcullen and David Brice for preparation of pastes specimens, John Gehman for his assistance in NMR data collection and Volker Rose and Xianghui Xiao for assistance in the data collection and processing on the 2BM instrument. Use of the Advanced Photon Source was supported by the U.S. Department of Energy, Office of Science, Office of Basic Energy Sciences, under Contract DE-AC02-06CH11357. The work of JLP and SAB received funding from the European Research Council under the European Union's Seventh Framework Programme (FP/2007-2013) / ERC Grant Agreement #335928 (GeopolyConc), and from the University of Sheffield.

References

1. van Deventer JSJ, Provis JL, Duxson P (2012) Technical and commercial progress in the adoption of geopolymer cement. Miner Eng 29:89-104.
2. Provis JL, van Deventer JSJ, eds. *Alkali-Activated Materials: State-of-the-Art Report, RILEM TC 224-AAM*. 2014, Springer/RILEM: Dordrecht.
3. Provis JL (2014) Green concrete or red herring? – the future of alkali-activated materials. Adv Appl Ceram:in press.
4. Provis JL (2014) Geopolymers and other alkali activated materials - Why, how, and what? Mater Struct 47(1):11-25.
5. Wang S-D, Pu X-C, Scrivener KL, Pratt PL (1995) Alkali-activated slag cement and concrete: a review of properties and problems. Adv Cem Res 7(27):93-102.
6. Puertas F (1995) Cementos de escoria activados alcalinamente: situación actual y perspectivas de futuro. Mater Constr 45(239):53-64.
7. Juenger MCG, Winnefeld F, Provis JL, Ideker J (2011) Advances in alternative cementitious binders. Cem Concr Res 41(12):1232-1243.
8. Duxson P, Provis JL (2008) Designing precursors for geopolymer cements. J Am Ceram Soc 91(12):3864-3869.
9. Shi C, Krivenko PV, Roy DM. Alkali-Activated Cements and Concretes, Abingdon, UK: Taylor & Francis, 2006.
10. Provis JL, Bernal SA (2014) Geopolymers and related alkali-activated materials. Annu Rev Mater Res:in press, DOI 10.1146/annurev-matsci-070813-113515.
11. Wang SD, Scrivener KL, Pratt PL (1994) Factors affecting the strength of alkali-activated slag. Cem Concr Res 24(6):1033-1043.
12. Živica V (2007) Effects of type and dosage of alkaline activator and temperature on the properties of alkali-activated slag mixtures. Constr Build Mater 21(7):1463-1469.
13. Fernández-Jiménez A, Puertas F (2003) Effect of activator mix on the hydration and strength behaviour of alkali-activated slag cements. Adv Cem Res 15(3):129-136.
14. Shi C, On the state and role of alkalis during the activation of alkali-activated slag cement, *Proceedings of the 11th International Congress on the Chemistry of Cement*, Durban, South Africa, 2003.

15. Song S, Sohn D, Jennings HM, Mason TO (2000) Hydration of alkali-activated ground granulated blast furnace slag. J Mater Sci 35:249-257.
16. Zhou H, Wu X, Xu Z, Tang M (1993) Kinetic study on hydration of alkali-activated slag. Cem Concr Res 23(6):1253-1258.
17. Puertas F, Martínez-Ramírez S, Alonso S, Vázquez E (2000) Alkali-activated fly ash/slag cement. Strength behaviour and hydration products. Cem Concr Res 30:1625-1632.
18. Ben Haha M, Le Saout G, Winnefeld F, Lothenbach B (2011) Influence of activator type on hydration kinetics, hydrate assemblage and microstructural development of alkali activated blast-furnace slags. Cem Concr Res 41(3):301-310.
19. Kashani A, Provis JL, Qiao GG, van Deventer JSJ (2014) The interrelationship between surface chemistry and rheology in alkali activated slag paste. Constr Build Mater:submitted for publication.
20. Krivenko PV. Alkaline cements. In: Krivenko PV, ed. Proceedings of the First International Conference on Alkaline Cements and Concretes. Kiev, Ukraine, VIPOL Stock Company, 1994. 11-129.
21. Xu H, Provis JL, van Deventer JSJ, Krivenko PV (2008) Characterization of aged slag concretes. ACI Mater J 105(2):131-139.
22. Provis JL, Duxson P, Kavalerova E, Krivenko PV, Pan Z, Puertas F, van Deventer JSJ. Historical aspects and overview. In: Provis JL, van Deventer JSJ, Alkali-Activated Materials: State-of-the-Art Report, RILEM TC 224-AAM, Springer/RILEM, Dordrecht. 2014, p. 11-57.
23. Provis JL, Brice DG, Buchwald A, Duxson P, Kavalerova E, Krivenko PV, Shi C, van Deventer JSJ, Wiercx JALM. Demonstration projects and applications in building and civil infrastructure. In: Provis JL, van Deventer JSJ, Alkali-Activated Materials: State-of-the-Art Report, RILEM TC 224-AAM, Springer/RILEM, Dordrecht. 2014, p. 309-338.
24. Moseson AJ, Moseson DE, Barsoum MW (2012) High volume limestone alkali-activated cement developed by design of experiment. Cem Concr Compos 34(3):328-336.
25. Sakulich AR, Miller S, Barsoum MW (2010) Chemical and microstructural characterization of 20-month-old alkali-activated slag cements. J Am Ceram Soc 93(6):1741-1748.
26. Moseson AJ. Design and Implementation of Alkali Activated Cement for Sustainable Development. Ph.D. Thesis, Drexel University, 2011.
27. Bai Y, Collier N, Milestone N, Yang C (2011) The potential for using slags activated with near neutral salts as immobilisation matrices for nuclear wastes containing reactive metals. J Nucl Mater 413(3):183-192.
28. Bakharev T, Sanjayan JG, Cheng Y-B (1999) Alkali activation of Australian slag cements. Cem Concr Res 29(1):113-120.
29. Fernández-Jiménez A, Puertas F (2001) Setting of alkali-activated slag cement. Influence of activator nature. Adv Cem Res 13(3):115-121.
30. Duran Atiş C, Bilim C, Çelik Ö, Karahan O (2009) Influence of activator on the strength and drying shrinkage of alkali-activated slag mortar. Constr Build Mater 23(1):548-555.
31. Fernández-Jiménez A, Puertas F, Sobrados I, Sanz J (2003) Structure of calcium silicate hydrates formed in alkaline-activated slag: Influence of the type of alkaline activator. J Am Ceram Soc 86(8):1389-1394.
32. Wang YX, De Carlo F, Mancini DC, McNulty I, Tieman B, Bresnahan J, Foster I, Insley J, Lane P, von Laszewski G, Kesselman C, Su MH, Thiebaux M (2001) A high-

throughput x-ray microtomography system at the Advanced Photon Source. Rev Sci Instrum 72(4):2062-2068.

33. Provis JL, Myers RJ, White CE, Rose V, van Deventer JSJ (2012) X-ray microtomography shows pore structure and tortuosity in alkali-activated binders. Cem Concr Res 42(6):855-864.
34. Fernandez-Jimenez A, Puertas F, Arteaga A (1998) Determination of kinetic equations of alkaline activation of blast furnace slag by means of calorimetric data. J Thermal Anal Calorim 52(3):945-955.
35. Bernal SA, San Nicolas R, Myers RJ, Mejía de Gutiérrez R, Puertas F, van Deventer JSJ, Provis JL (2014) MgO content of slag controls phase evolution and structural changes induced by accelerated carbonation in alkali-activated binders. Cem Concr Res 57:33-43.
36. Ben Haha M, Lothenbach B, Le Saout G, Winnefeld F (2011) Influence of slag chemistry on the hydration of alkali-activated blast-furnace slag -- Part I: Effect of MgO. Cem Concr Res 41(9):955-963.
37. Bernal SA, Provis JL, Walkley B, San Nicolas R, Gehman J, Brice DG, Kilcullen A, Duxson P, van Deventer JSJ (2013) Gel nanostructure in alkali-activated binders based on slag and fly ash, and effects of accelerated carbonation. Cem Concr Res 53:127-144.
38. Bernal SA, Provis JL, Brice DG, Kilcullen A, Duxson P, van Deventer JSJ (2012) Accelerated carbonation testing of alkali-activated binders significantly underestimate the real service life: The role of the pore solution. Cem Concr Res 42(10):1317-1326.
39. Sun GK, Young JF, Kirkpatrick RJ (2006) The role of Al in C-S-H: NMR, XRD, and compositional results for precipitated samples. Cem Concr Res 36(1):18-29.
40. Bernal SA, San Nicolas R, Provis JL, Mejía de Gutiérrez R, van Deventer JSJ (2014) Natural carbonation of aged alkali-activated slag concretes. Mater Struct DOI:10.1617/s11527-11013-10089-11522.
41. Escalante-Garcia J, Fuentes AF, Gorokhovsky A, Fraire-Luna PE, Mendoza-Suarez G (2003) Hydration products and reactivity of blast-furnace slag activated by various alkalis. J Am Ceram Soc 86(12):2148-2153.
42. Bernal SA, Provis JL, Mejía de Gutiérrez R, van Deventer JSJ (2014) Accelerated carbonation testing of alkali-activated slag/metakaolin blended concretes: effect of exposure conditions. Mater Struct:in press.
43. Le Saoût G, Ben Haha M, Winnefeld F, Lothenbach B (2011) Hydration degree of alkali-activated slags: A ^{29}Si NMR study. J Am Ceram Soc 94(12):4541-4547.
44. Benharrats N, Belbachir M, Legrand AP, D'Espinose de la Caillerie J-B (2003) ^{29}Si and ^{27}Al MAS NMR study of the zeolitization of kaolin by alkali leaching. Clay Miner 38(1):49-61.
45. Ward RL, McKague HL (1994) Clinoptilolite and heulandite structural differences as revealed by multinuclear nuclear magnetic resonance spectroscopy. J Phys Chem 98(4):1232-1237.
46. Richardson IG, Brough AR, Brydson R, Groves GW, Dobson CM (1993) Location of aluminum in substituted calcium silicate hydrate (C-S-H) gels as determined by ^{29}Si and ^{27}Al NMR and EELS. J Am Ceram Soc 76(9):2285-2288.
47. Andersen MD, Jakobsen HJ, Skibsted J (2003) Incorporation of aluminum in the calcium silicate hydrate (C−S−H) of hydrated Portland cements: A high-field ^{27}Al and ^{29}Si MAS NMR investigation. Inorg Chem 42(7):2280-2287.
48. Ben Haha M, Lothenbach B, Le Saout G, Winnefeld F (2012) Influence of slag chemistry on the hydration of alkali-activated blast-furnace slag -- Part II: Effect of Al_2O_3. Cem Concr Res 42(1):74-83.

643 49. Myers RJ, Bernal SA, San Nicolas R, Provis JL (2013) Generalized structural
644 description of calcium-sodium aluminosilicate hydrate gels: The crosslinked
645 substituted tobermorite model. Langmuir 29(17):5294-5306.
646 50. Bernal SA, Provis JL, Walkley B, San Nicolas R, Gehman JD, Brice DG, Kilcullen A,
647 Duxson P, van Deventer JSJ (2013) Gel nanostructure in alkali-activated binders based
648 on slag and fly ash, and effects of accelerated carbonation. Cem Concr Res 53:127-144.
649 51. Engelhardt G, Michel D. High-Resolution Solid-State NMR of Silicates and Zeolites,
650 Chichester: John Wiley & Sons, 1987.
651 52. Ward RL, McKague HL (1994) Clinoptilolite and heulandite structural differences as
652 revealed by multinuclear nuclear magnetic resonance spectroscopy. J Phys Chem
653 98(4):1232-1237.
654 53. Valentini L, Dalconi MC, Parisatto M, Cruciani G, Artioli G (2011) Towards three-
655 dimensional quantitative reconstruction of cement microstructure by X-ray diffraction
656 microtomography. J Appl Cryst 44:272-280.
657 54. Sugiyama T, Promentilla MAB, Hitomi T, Takeda N (2010) Application of synchrotron
658 microtomography for pore structure characterization of deteriorated cementitious
659 materials due to leaching. Cem Concr Res 40(8):1265-1270.
660
661